

# Pitfalls in using statistical bias-correction methods to characterize climate change impacts

Nicolás A. Vásquez<sup>1</sup>, Pablo A. Mendoza<sup>1,2</sup>, Wouter J. M. Knoben<sup>3\*</sup>, Louise Arnal<sup>3†</sup>, Miguel Lagos-Zúñiga<sup>4</sup>, Martyn Clark<sup>3‡</sup>, Ximena Vargas<sup>1</sup>

<sup>1</sup>Department of Civil Engineering, Universidad de Chile

<sup>2</sup>Advanced Mining Technology Center, Universidad de Chile

<sup>3</sup>Centre for Hydrology, University of Saskatchewan, Canmore, Alberta, Canada

<sup>4</sup>Center for Climate and Resilience Research, Universidad de Chile

## Key Points:

- The choice of temporal stratification for GCM bias correction is crucial for removing biases, even for GCMs with good raw seasonality.
- Different temporal stratifications used for GCM bias correction may yield different future seasonalities and signals in projected changes.
- The scaling factor method is effective to assess if the temporal stratification affects the precipitation seasonality projected by a GCM.

---

\*now at the Department of Civil Engineering, Schulich School of Engineering, University of Calgary, Calgary, Alberta, Canada

†now at Ouranos, Montreal, Quebec, Canada

‡now at the Department of Civil Engineering, Schulich School of Engineering, University of Calgary, Calgary, Alberta, Canada

Corresponding author: Nicolás A. Vásquez, [nicolas.vasquez.p1@uchile.cl](mailto:nicolas.vasquez.p1@uchile.cl)

16      **Abstract**

17      Characterizing climate change impacts on water resources typically relies on Global Climate Model (GCM) outputs that are bias-corrected using observational datasets. In this  
 18      process, two pivotal decisions are (i) the Bias Correction Method (BCM) and (ii) how  
 19      to handle the historically observed time series, which can be used as a continuous whole  
 20      (i.e., without dividing it into sub-periods), or partitioned into monthly, seasonal (e.g.,  
 21      three months), or any other temporal stratification (TS). Here, we examine how the in-  
 22      terplay between the choice of BCM, TS, and the raw GCM seasonality may affect his-  
 23      torical portrayals and projected changes. To this end, we use outputs from 29 GCMs be-  
 24      longing to the CMIP6 under the Shared Socioeconomic Pathway 5–8.5 scenario, using  
 25      seven BCMS and three TSs (entire period, seasonal, and monthly). The results show that  
 26      the effectiveness of BCMS in removing biases can vary depending on the TS and climate  
 27      indices analyzed. Further, the choice of BCM and TS may yield different projected change  
 28      signals and seasonality (especially for precipitation), even for climate models with low  
 29      bias and a reasonable representation of precipitation seasonality during a reference pe-  
 30      riod. Because some BCMS may be computationally expensive, we recommend using the  
 31      linear scaling method as a diagnostics tool to assess how the choice of TS may affect the  
 32      projected precipitation seasonality of a specific GCM. More generally, the results pre-  
 33      sented here unveil trade-offs in the way BCMS are applied, regardless of the climate regime,  
 34      urging the hydroclimate community for a careful implementation of these techniques.  
 35

36      **Plain Language Summary**

37      Global Climate Models (GCMs) are useful tools to characterize the historical and  
 38      future evolution of the Earth's climate and its impacts on water resources. Because these  
 39      models contain errors and their horizontal resolution is too coarse for local impact as-  
 40      sessments, spatial downscaling and bias correction are required steps. In particular, bias  
 41      correction methods can be trained and applied using all the available historical data or  
 42      by splitting the time series (e.g., by season or months). Since there is no guideline on  
 43      selecting a temporal stratification, we analyze bias-corrected GCM outputs obtained with  
 44      three types of strategy (entire period, seasons, and months) and seven bias-correction  
 45      techniques over continental Chile. We show that the choice of bias correction method  
 46      and the temporal stratification applied can modify the projected precipitation signal and  
 47      seasonality. We also propose a simple statistical technique to identify if, for a given cli-  
 48      mate model, the temporal stratification may be a relevant decision for climate impact  
 49      assessments.

50      **1 Introduction**

51      Understanding and quantifying climate change impacts is crucial for long-term wa-  
 52      ter resources planning and management. Such characterization typically involves hydro-  
 53      logic model simulations forced by an ensemble of scenario-driven meteorological time se-  
 54      ries obtained from Statistically Downscaled Bias-Corrected (SDBC) Global Climate Model  
 55      (GCM) outputs (e.g., Addor et al., 2014; Hattermann et al., 2018; Her et al., 2019; Chen  
 56      et al., 2021; Hanus et al., 2021; Vicuña et al., 2021). This approach usually requires the  
 57      choice of emission scenario (e.g., Vano et al., 2015; Chegwidden et al., 2019), the choice  
 58      of GCM (e.g., Hakala et al., 2018; Di Virgilio et al., 2022), the selection of Bias Correc-  
 59      tion Method (BCM) (e.g., Werner & Cannon, 2016; Gutiérrez et al., 2019; Hess et al.,  
 60      2023), and the choice of observational (or reference) dataset (e.g., Wootten et al., 2021;  
 61      Rastogi et al., 2022).

62      Among the above decisions, the selection and configuration of BCMS is a critical  
 63      step given the risk of introducing artificial perturbations in GCM outputs (Hagemann  
 64      et al., 2011; Maurer & Pierce, 2014; Wootten et al., 2021), generating a mismatch be-  
 65      tween simulated (i.e., obtained from bias-corrected GCMs) and observed (i.e., obtained

from a reference dataset) annual cycles of climate variables (e.g., precipitation; Deutschbein & Seibert, 2010; Alder & Hostetler, 2019; Chen et al., 2021), with potential effects on projected climate change impacts and subsequent interpretations and adaptation strategies. A somewhat overlooked step is the strategy for handling the time series when applying BCMs, hereafter referred to as temporal stratification (TS). For example, the bias correction of simulated daily time series can be performed using all the historical period (i.e., a single application of the BCM; e.g., Ghimire et al., 2019) or sub-periods of the historical time series, such as seasons (e.g., four applications of the BCM; e.g., Ruffault et al., 2014; Teng et al., 2015), months (i.e., twelve applications of the BCM; e.g., Pierce et al., 2015; Switanek et al., 2017; Matiu & Hanzer, 2022; Wu et al., 2022; J. Guo et al., 2023), or any other temporal window (e.g., Haerter et al., 2011; Reiter et al., 2018).

Despite the large body of work exploring modeling decisions at the top of the ‘cascade of uncertainty’ (Wilby & Dessai, 2010), climate impact studies have typically relied on subjectively selected TSs. For example, Teng et al. (2015) compared four BCMs (applied with a seasonal TS) for hydrological projections in southeastern Australia, concluding that the hydrological model amplifies biases in precipitation after applying the BCMs, and that the large spread in the projected signal of changes in precipitation extremes yields different impacts on runoff. Hakala et al. (2018) applied the quantile mapping (QM) method (using a seasonal TS) to assess whether a hydrological model, forced by SDBC GCMs, can replicate the hydrological climatology observed during a historical reference period, obtaining that, even after bias correction, biases in precipitation and streamflow seasonality persist. To analyze the effects of different observational datasets and BCMs on climate projections, Wootten et al. (2021) used three observational datasets to apply two BCMs: (i) the ‘Delta’ approach with a 3-month moving window, and (ii) the quantile delta mapping (QDM) method over four periods consisting of three non-overlapping months. They concluded that the selection of BCMs and observational datasets have different impacts on historical and projected time series for different variables, although they did not isolate the effect of the TS.

Other studies have focused on the ability of different BCMs to reproduce historically observed climate indices (e.g., Gutmann et al., 2014; François et al., 2020; Xavier et al., 2022), or the effects on climate projections (e.g., Maurer & Pierce, 2014; Melsen et al., 2018), without emphasizing the role of the TS and the evaluation timescale. More recently, Vogel et al. (2023) proposed a framework to evaluate downscaling and BCMs for climate change studies and demonstrated it over Australia using four GCMs, three BCMs and two downscaling methods, considering different TS (monthly, 3-month, and multi-time scales) for the BCMs. They suggested that the TS may influence the analysis (after bias correction) and should be adequately chosen after a careful bias assessment.

Although the preceding studies have covered domains with specific climate types, the trade-offs in selecting TS, BCMs, and GCMs for estimating historical biases (after applying BCMs) and projections across contrasting climates remain unclear. Hence, this paper seeks to disentangle the relative contribution of these decisions (especially TS) to the spread of bias-corrected time series at the annual, seasonal, and monthly timescales during historical and future periods rather than finding the ‘best’ configuration for the assessment of climate change impacts. Specifically, we address the following research questions:

1. To what extent does the choice of bias correction method and temporal stratification alter historical GCM simulations across different climate regions?
2. What are the effects of bias correction methods and temporal stratification on the projected signal and seasonality of different climate variables?

- 116        3. Are there any connections between the effects of TS (on historical biases and pro-  
 117        jections) and the capability of raw GCM output to replicate historically observed  
 118        climatology?

119        To seek answers, we evaluate the performance of 29 SDBC GCMs from the sixth phase  
 120        of the Coupled Models Intercomparison Project (CMIP6; O'Neill et al., 2016) over dif-  
 121        ferent climate groups in continental Chile. We use seven methods (three univariate and  
 122        four multivariate) to correct biases in precipitation and maximum and minimum tem-  
 123        perature. All BCMs are applied at three different TSs: (i) using the entire period (i.e.,  
 124        all daily data simultaneously used for one application of the BCM), (ii) seasonally (i.e.,  
 125        four applications of the BCM using four seasonally stratified time series), and (iii) monthly  
 126        (i.e., twelve applications of the BCM for twelve monthly stratified time series).

## 127        2 Study area and datasets

### 128        2.1 Study area

129        Our study domain is continental Chile, which is suitable for a comprehensive as-  
 130        sessment of the TS-BCM-GCM interplay in very different climate types. Figure 1 shows  
 131        the spatial distribution of mean annual precipitation, mean annual temperature, and three  
 132        climate indices. The snowfall fraction  $SF = Sn/P$  (Figure 1d) is the fraction of mean  
 133        annual precipitation ( $P$ , Figure 1b) falling as snow ( $Sn$ ). The aridity index (Figure 1e)  
 134        is the ratio between mean annual potential evapotranspiration ( $PET$ ) and mean annual  
 135        precipitation. Finally, the precipitation seasonality (p-seasonality, Figure 1f) indicates  
 136        whether most precipitation falls during winter (negative values) or summer (positive val-  
 137        ues). In this paper, we use the season names within the context of the Southern Hemis-  
 138        phere (i.e., winter refers to months JJA, while summer to DJF).

139        In the northern area ( $17^{\circ}\text{S}$ - $25^{\circ}\text{S}$ ), two main climate zones can be identified: (i) the  
 140        super-arid coastal area, with very low annual precipitation amounts ( $<50 \text{ mm/yr}$ ), and  
 141        (ii) the Altiplano region, with lower temperatures due to increasing altitude and larger  
 142        annual precipitation ( $\sim 200 \text{ mm/yr}$ ). The mean annual precipitation increases towards  
 143        the south, although the Andes Cordillera generates a west-east gradient, with larger pre-  
 144        cipitation amounts and lower temperatures on the western slopes of the Andes Cordillera  
 145        compared to the valleys. Moving south from  $\sim 37^{\circ}\text{S}$ , the altitude of Andean mountains  
 146        progressively decreases, as well as the contribution of snowmelt to runoff, whereas pre-  
 147        cipitation increases. South from  $45^{\circ}\text{S}$ , a west-to-east precipitation gradient produces high  
 148        precipitation amounts on the coast ( $>2500 \text{ mm/yr}$ ), whereas a dry climate develops in  
 149        Patagonia a few kilometers to the east, with decreasing precipitation amounts. In sum-  
 150        mary: (i) most snowfall occurs in the Andes Cordillera, though snowfall events can also  
 151        occur in the valleys of Austral Chile ( $<45^{\circ}\text{S}$ ); (ii) the hydroclimate is water-limited ( $PET/P >$   
 152        1) in approximately half of the Chilean territory, especially from  $\sim 35^{\circ}\text{S}$  to the north, whereas  
 153        the hydroclimate of the south is energy limited ( $PET/P < 1$ ); and (iii) most precipi-  
 154        tation in Chile falls during the winter (red color in panel f), being the Altiplano (north-  
 155        ern Chile) and Patagonia ( $\sim 50\text{-}55^{\circ}\text{S}$ ) two notable exceptions. For a more comprehen-  
 156        sive review of the climate and weather of Chile, readers are referred to Aceituno et al.  
 157        (2021) and Vásquez et al. (2021).

### 158        2.2 Datasets

159        We use the gridded meteorological product CR2MET v2.5 (Boisier et al., 2018; DGA,  
 160        2022) as the observational baseline (hereafter reference dataset). CR2MET precipita-  
 161        tion estimates (pr) are obtained through a combination of (i) logistic regression mod-  
 162        els and (ii) multiple linear regression models that use ERA5 reanalysis outputs (Hersbach  
 163        et al., 2020) and geomorphological attributes as predictors and daily precipitation from  
 164        meteorological stations as predictands. For daily extreme temperatures (tmax and tmin),

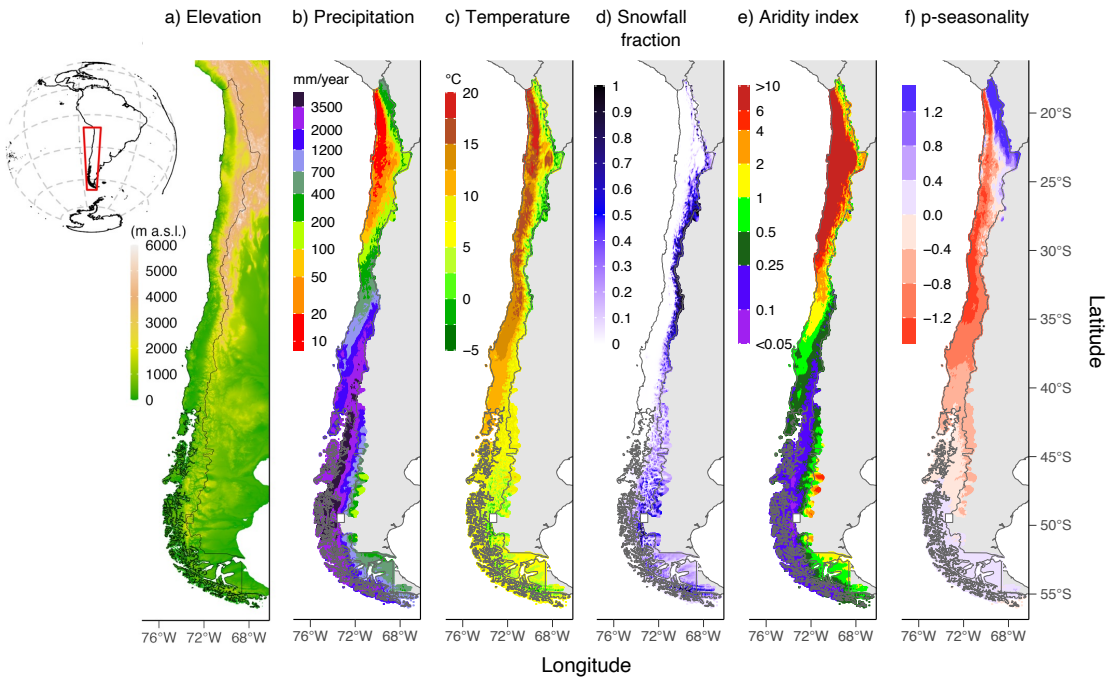


**Figure 1.** Main physiographic and climate attributes of continental Chile for the period 1980-2014 (34 water years): (a) elevation, (b) mean annual precipitation, (c) mean annual temperature, (d) snowfall fraction, (e) aridity index, and (f) p-seasonality.

land surface temperature from MODIS AQUA and TERRA (Wan, 2014) are also included as predictors. All variables (pr, tmax, and tmin) are available at a daily time step for the period January/1979–March/2020, covering continental Chile at a horizontal resolution of  $0.05^\circ \times 0.05^\circ$ . The mean daily temperature is computed as the average between tmax and tmin. It should be noted that CR2MET is, arguably, the most accurate meteorological dataset for continental Chile since its development incorporated local meteorological stations.

We use outputs from 29 GCMs from the CMIP6 (O'Neill et al., 2016), based on the data availability for pr, tmax and tmin during the historical and projected periods, and the SSP5-8.5 scenario for being the worst in terms of greenhouse emissions and the ‘business as usual’ development case. The name and horizontal resolution of each GCM are included in Table A1.

### 3 Methodology

Figure 2 shows the main steps of our approach. First, we delineate climate zones across Chile using cluster analysis (step 1), with the aim to examine possible relationships between climate types and the BCM-TS-GCM interplay. Step 2 considers different strategies for correcting biases in GCM outputs (i.e., seven bias-correction methods are applied using three different stratification periods). In step 3, we compute several climate indices derived from precipitation and temperature at different time scales (e.g., annual, seasonal, and monthly mean values), for a historical and a future period. Finally, we conduct an Analysis of Variance (ANOVA) to quantify the relative contribution of different decisions to the spread of historical estimates. More details can be found in the following sections.

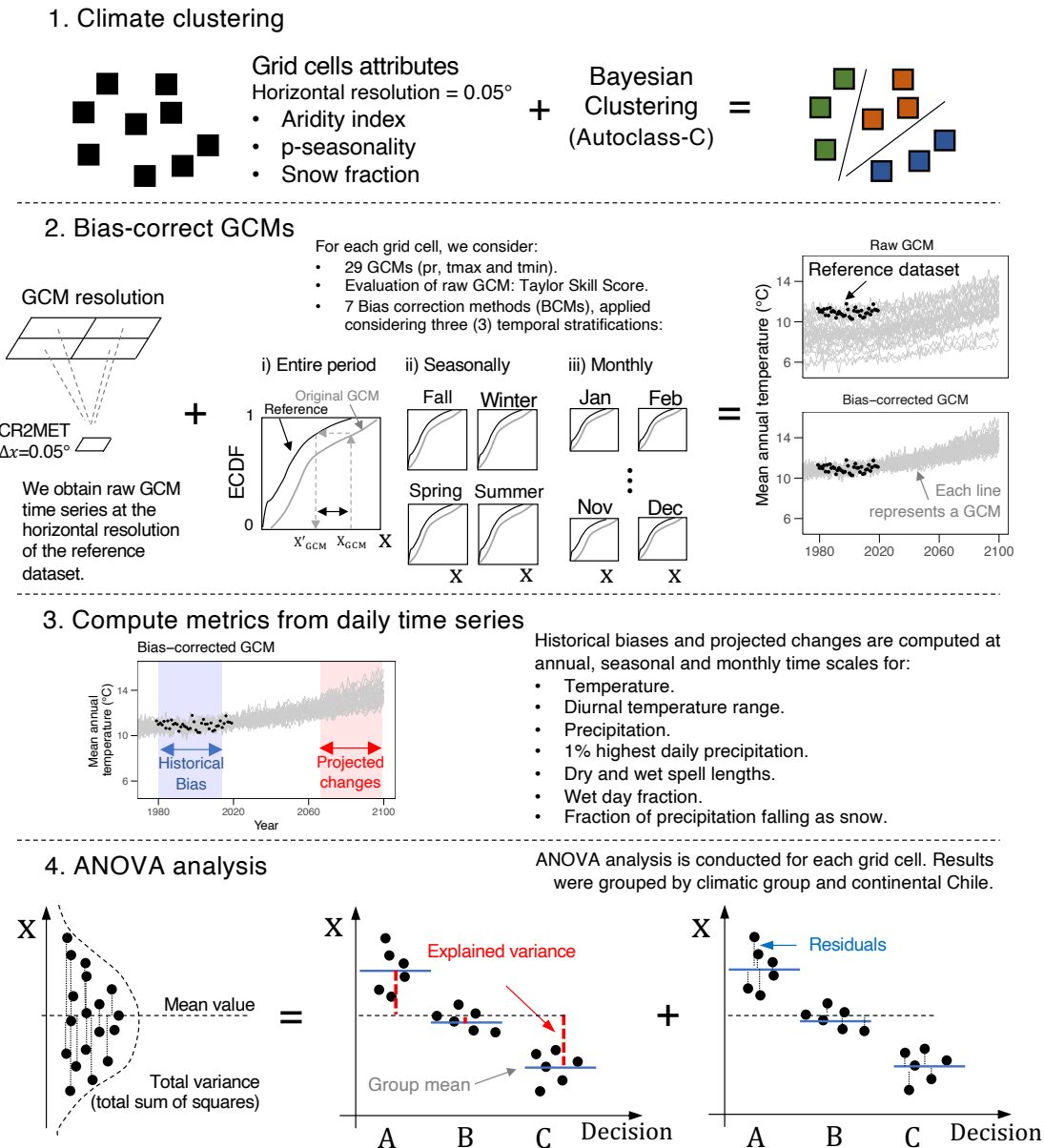


**Figure 2.** Diagram of the methodology used in this study

188      **3.1 Climate clustering**

189      We perform a Bayesian clustering to identify climate zones across Chile. To this  
 190      end, we use the aridity index ( $PET/P$ ), the p-seasonality, and the fraction of precipi-  
 191      tation falling as snow as explanatory variables, since they reflect observed hydrological  
 192      behaviors (Knoben et al., 2018).  $PET$  is computed using the Oudin et al. (2005) for-  
 193      mula - available in the R Package airGR (Coron et al., 2017) - which requires air tem-  
 194      perature (provided at daily time steps here) and latitude as inputs. To estimate  $Sn$ , we  
 195      consider that snowfall occurs when the mean daily temperature is below 2°C (Jennings  
 196      et al., 2018; Han et al., 2019; Sepúlveda et al., 2022), and p-seasonality is computed with  
 197      the formula proposed by Woods (2009).

198      Prior climate groups are defined with the Autoclass-C software (Cheeseman et al., 1988,  
 199      1996), which has been previously used in hydrological applications (e.g., Sawicz et al.,  
 200      2011). We subsequently refined the clustering results through visual inspection, group-  
 201      ing small clusters based on spatial proximity and climate similarity.

202      **3.2 Raw GCM performance**

203      We use the Taylor Skill Score (TSS; Taylor, 2001) to evaluate the role of the raw  
 204      GCM performance and its interplay with BCM and TS for SDBC-biases and projections  
 205      at different time scales. The TSS is computed at the grid cell level ( $0.05^\circ \times 0.05^\circ$ ) for the  
 206      period 1980-2014, contrasting downscaled GCM outputs against the reference dataset,  
 207      as is commonly done for local climate impact assessments (e.g., Lafon et al., 2013). In  
 208      this study, TSS is computed for precipitation, as shown in Eq. 1.

$$209 \quad TSS = \frac{4(1 + R)}{\left(\hat{\sigma} + \frac{1}{\hat{\sigma}}\right)^2 (1 + R_o)} \quad (1)$$

210      where  $R$  is the Pearson correlation coefficient between the raw GCM and the reference  
 211      mean seasonality, and  $\hat{\sigma} = \sigma_{GCM}/\sigma_{REF}$  is the ratio between the standard deviation  
 212      of raw monthly values ( $\sigma_{GCM}$ ) and the reference ( $\sigma_{REF}$ ).  $R$ , and  $\hat{\sigma}$  are computed us-  
 213      ing simulated and observed mean monthly values of each variable (i.e., 12 values of GCMs  
 214      vs. 12 reference values).  $R_o$  is the maximum achievable Pearson correlation coefficient  
 215      for a specific GCM, which is assumed to be  $R_o \cong 1$  to simplify the analysis. When  $R \rightarrow$   
 216       $R_o$  and  $\hat{\sigma} \rightarrow 1$ , the  $TSS \rightarrow 1$ . Alternatively,  $TSS \rightarrow 0$  when  $R$  decreases or  $\hat{\sigma}$  ap-  
 217      proaches zero or infinity. Hence,  $TSS$  ranges between 0 and 1. Further, we compute the  
 218       $TSS$  for each climate group, estimating the mean group climatology through spatial av-  
 219      erages.

220      **3.3 Bias correction of GCMs**

221      **3.3.1 Bias correction methods**

222      We downscale the raw GCM outputs to the CR2MET grid using inverse distance  
 223      weighting, considering the four closest GCM grid cells. We use seven bias correction meth-  
 224      ods, including three univariate and four multivariate techniques, listed in Table 1 and  
 225      briefly reviewed here. The quantile delta mapping (QDM) preserves the projected change  
 226      for each quantile while correcting the bias. Empirical cumulative density functions are  
 227      estimated for the historical reference ( $F_{h,ref}$ ), the raw historical GCM ( $F_{h,GCM}$ ), and  
 228      the raw projected GCM ( $F_{p,GCM}$ ) to relate ( $X$ ) with the cumulative probability ( $\tau$ ). For  
 229      a specific value during the historical period  $X_{h,GCM}$ , the correction (for pr) is given by  
 230       $X'_{h,GCM} = F_{h,ref}^{-1}(F_{h,GCM}(X_{h,GCM}))$ , while for a projected raw GCM value  $X_{p,GCM}$ ,  
 231      the corrected value is  $X'_{p,GCM} = \Delta \cdot F_{h,GCM}^{-1}(F_{p,GCM}(X_{p,GCM}))$ , where  $\Delta$  is computed  
 232      as  $\Delta = X_{p,GCM}/F_{h,GCM}^{-1}(F_{p,GCM}(X_{p,GCM}))$  for precipitation.  
 233      The asynchronous regression (AR) relies on a piecewise linear regression calibrated with  
 234      sorted raw GCM and reference data during a historical period (i.e.,  $F_{h,ref}$  is a function  
 235      of  $F_{h,GCM}$ ). Although a simple linear regression could be used, the error in the tails of

the regression can be large and, therefore, the data is split by including different knots (up to six) to reduce errors in low and high values. To bias-correct projected values, the calibrated piecewise linear regression is applied. The quantile regressions neural network (QRNN) uses neural networks to bias correct the sorted data (i.e., quantiles) from simulations and the reference. QRNN is a flexible model since it does not assume a specific relationship between the raw GCM and the reference data.

The rank resampling for distributions and dependences ( $R^2D^2$ ) corrects the covariance among sites and/or variables through four steps: (i) the univariate bias correction of each variable/site separately, (ii) the selection of one variable/site and the computation of the ranking for all variables/sites, (iii) for a specific date, select the same ranking in the reference period for the dimension selected, and (iv) the shuffling of the other variables/sites to maintain rank structure.

The ‘multivariate bias correction’ family (MBC) includes three different methods using the Pearson correlation coefficient (MBCp), the Spearman rank correlation coefficient (MBCr), and an N-dimensional probability density function (MBCn) to transform the raw correlated GCM data (i.e., the intervariable dependence structure) through consecutive iterations. For MBCp and MBCr, the transformation relies on the Cholesky matrix decomposition and the correction of the covariance matrix. Conversely, MBCn relies on an orthogonal rotation, the application of QDM to these orthogonal variables, and, finally, the application of an inverse matrix (the one used to compute the orthogonal variables) to obtain the resulting data. The reader is referred to the studies listed in Table 1 for more details on the methods.

**Table 1.** Methods considered in this study to bias-correct GCMs outputs (pr, tmax, and tmin).

Acronym	Name	Type	Reference
QDM	Quantile Delta Mapping		Cannon et al. (2015)
AR	Asynchronous Regression	Univariate	Dettinger et al. (2004); Stoner et al. (2013)
QRNN	Quantile Regression Neural Network		Cannon (2011)
$R^2D^2$	Rank Resampling for Distributions and Dependences		Vrac and Thao (2020)
MBCp	Multivariate Bias Correction method - Pearson		
MBCr	Multivariate Bias Correction method - Rank	Multivariate	Cannon (2016)
MBCn	Multivariate Bias Correction method – QDM		Cannon (2018)

We stress that it is not our aim to perform detailed comparisons among different bias correction techniques but to quantify the impact of this and other methodological choices on historical biases and projected changes in climate indices. All bias correction methods were applied using the statistical software ‘R’ (<http://www.r-project.org/>). The QDM, MBCp, MBCr, MBCn, and  $R^2D^2$  methods were applied using the library ‘MBC’ (Cannon, 2018). QRNN was implemented using the ‘qrnn’ library (also available in R), while the AR method was implemented following Stoner et al. (2013). To reduce the computational effort, we randomly select 100 grid cells within each climate group, and all subsequent analyses are conducted at these grid cells ( $100 \cdot N_{clusters}$ ).

### 3.3.2 Choice of the temporal stratification

Bias correction methods can be applied using different stratification strategies. For example, a BCM can be applied at daily time steps using all the data in the historical period (usually 30 years), which means that all  $\sim 10,950$  days ( $\sim 365$  days  $\cdot$  30 years) are simultaneously bias-corrected. For a seasonal TS, BCMs are applied four times, each one considering  $\sim 2730$  days ( $\sim 91$  days  $\cdot$  30 years), whereas for a monthly TS, the BCM is applied 12 times considering  $\sim 900$  days ( $\sim 30$  days  $\cdot$  30 years). Note that other tempo-

ral stratifications could be considered. Here, we applied BCMs to daily time series of pr, tmax, and tmin (e.g., Rastogi et al., 2022) using the entire time series in the historical period (1980-2014), and stratifying the data seasonally and monthly, since these TSs are typically considered for climate change impact assessments. For all combinations of BCM and TS, we obtained daily time series from 1980 to 2100.

### 279      3.4 Climate indices

We consider several climate indices that are relevant to reproduce historically observed hydrological responses (e.g., Gutmann et al., 2014), including (i) mean annual, seasonal, and monthly total precipitation, (ii) highest 1% daily precipitation, (iii), wet-day fraction, (iv) wet and dry-spell lengths, (v) fraction of precipitation falling as snow, and (vi) annual, seasonal and monthly averages of mean daily temperature and diurnal temperature ranges. To estimate the mean annual snowfall, we add all precipitation amounts for days with a mean daily temperature below 2°C. Wet-spell and dry-spell lengths (mean consecutive rainy and non-rainy days, respectively), as well as the wet-day fraction (mean fraction of rainy days) are computed as in Gutmann et al. (2014), considering 0.1 mm/d as a threshold. To examine the capability of BCMs to replicate historically observed climate indices, we computed the difference between SDBC-GCM outputs and the reference dataset during the historical period 1980-2014 as a percent bias (hereafter referred to as biases). Additionally, we analyze the effects of BCMs on climate projections by computing the relative change for the period 2065-2099 with respect to the historical period (1980-2014).

### 295      3.5 Analysis of Variance

To evaluate the relative contribution of the BCM and TS decisions to the spread of SDBC-biases we perform, for each combination of GCM and grid cell, an analysis of variance (ANOVA). In this case, the ANOVA is simplified as:

$$299 \quad TV = BCM + AP + Residual \quad (2)$$

where TV stands for the total variance of SDBC-biases, and the residual term is the variance not explained by the BCM nor the TS for a specific GCM-grid cell combination. If the choice of TS had no impact on the biases in climate indices. In that case, the application of Supposey BCM should be able to reduce biases at all temporal scales (e.g., annual, seasonal, or monthly), regardless of the GCM considered. To summarize the information at the grid cell level, we compute the average of  $BCM/TV$ ,  $TS/TV$ , and  $Residual/TV$  fractions across GCMs, whereas for the climate groups, we compute the mean relative contribution (estimated by  $BCM/TV$ ,  $TS/TV$  and  $Residual/TV$ ) of TS and BCM to the spread as the average of fractions across the grid cells within that group.

## 309      4 Results

We show the climate clustering results, the historical biases after applying the BCMs, and the relative contributions of different methodological choices to historical biases of climate indices at the annual and seasonal scales. Further, we include the TSS performance to examine connections between the raw seasonality of the GCMs and the selection of BCM and TS. For simplicity, we only show the results for precipitation, and the remaining variables can be found in the Supporting Information.

### 316      4.1 Clustering

The Bayesian clustering and subsequent spatial aggregation through visual inspection provided ten climate groups for continental Chile (Figure 3). In general, the clusters follow two main climate patterns in Chile: (i) a latitudinal precipitation gradient,

320 from very arid (north) to humid (south), and (ii) a west-east gradient from the coast to  
 321 the Andes Cordillera. Although northern Chile encloses groups 1, 2, and 3, clusters 2  
 322 and 3 are located in the Altiplano region, where larger precipitation and lower temper-  
 323 atures are observed. Groups 5, 6, and 8 span the coast and valley, whereas groups 4 and  
 324 7 are located in the Andes. Finally, groups 9 (the雨iest group) and 10 are in south-  
 325 ern Chile, characterized by large precipitation amounts in the Andes Cordillera and the  
 326 coast, with decreasing precipitation and temperature towards the east (Patagonia).

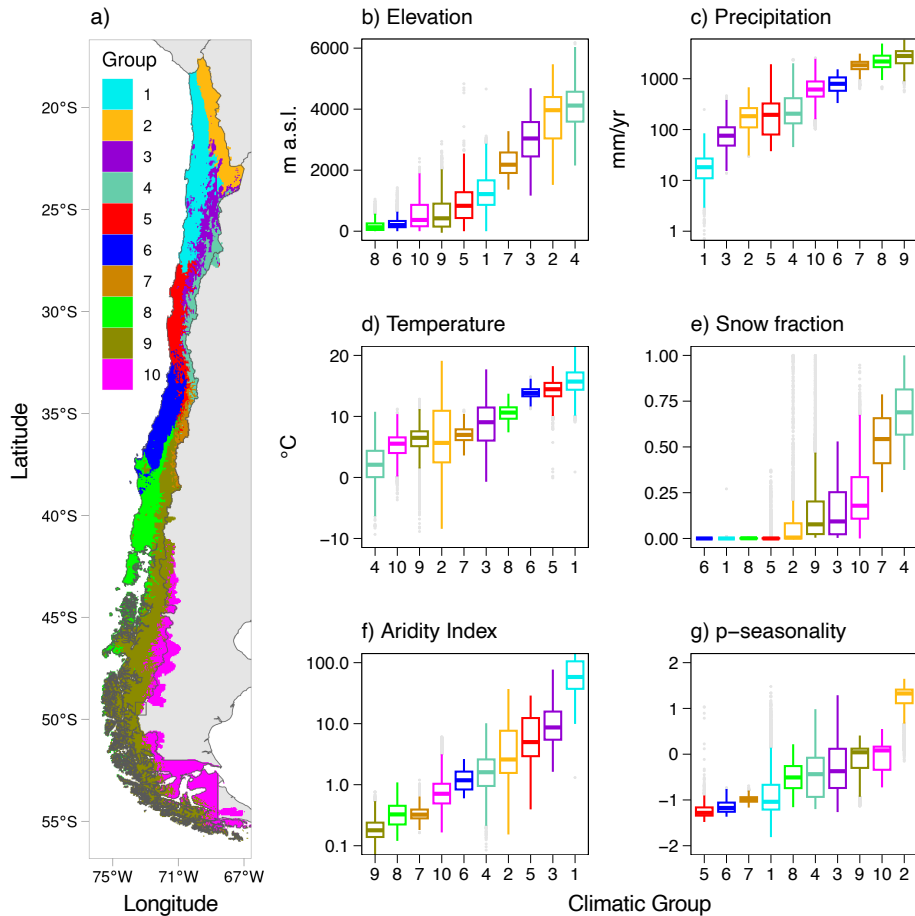


**Figure 3.** (a) Spatial distribution of climate clusters in continental Chile based on snowfall fraction, aridity index, and p-seasonality. The following attributes are ordered by the median of each group: (b) elevation, (c) precipitation, (d) temperature, (e) snowfall fraction, (f) aridity index, and (g) p-seasonality. All climate indices were computed for the period 1980-2014. Notice that the boxplots in panels b-g are sorted according to the median value, and the group's order on the x-axis differs among variables.

327

#### 4.2 Performance metrics after bias correction

328

Figure 4 shows precipitation biases (after bias correction) in three different climate groups (the other variables and climate groups can be found in the Supporting Information). The results show that, regardless of the combination of GCM, BCM, TS and grid cell, biases in annual amounts are close to zero (Figure 4a). When the BCM is applied

329

330

331

332 using all the data in the historical period (Figure 4b, left), biases in monthly precipitation  
 333 amounts can be large, although the magnitude varies among climate groups. In climate group 2 (Altiplano region), precipitation occurs mostly during the summer (DJF);  
 334 in this season, the median bias associated with January precipitation is relatively lower  
 335 - though still considerable (>20%) - compared to the remaining months. In group 6, most  
 336 precipitation occurs during the winter (JJA), and biases can be found in any month. In  
 337 group 10, precipitation falls uniformly throughout the year, with slightly larger amounts  
 338 and larger biases during the summer (DJF). When the BCM is applied seasonally (4b,  
 339 center), monthly precipitation biases persist. However, these are generally lower com-  
 340 pared to the case when the bias correction is applied using the entire dataset, especially  
 341 in climate group 10. As expected, biases are nearly removed with a monthly TS (Fig-  
 342 ure 4b, right), regardless of the GCM, bias correction method, grid cell, or climate group.  
 343

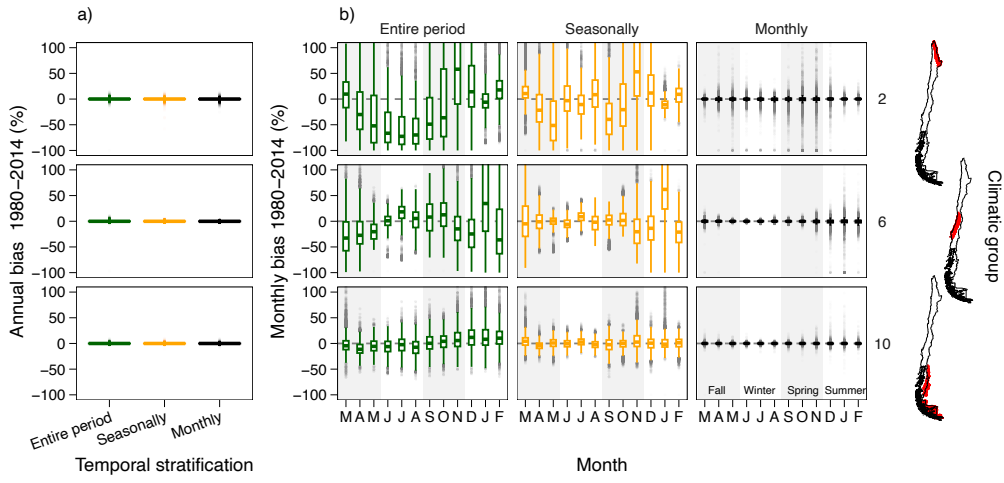


**Figure 4.** Historical biases in precipitation at the (a) annual and (b) seasonal time scales in three climate groups (rows) after applying the BCMs. The columns in panel b) show results for the three TSs used to apply the BCMs. Each boxplot comprises results from the 100 grid cells within a specific climate group, 29 GCMs, and seven BCMS. The different seasons are highlighted through grey-white areas.

344 Figure 5 displays the relative contributions of the BCM, TS, and residuals for mean  
 345 annual, seasonal (summer and winter), and monthly (January and July) precipitation  
 346 biases averaged across 1,000 grid cells in continental Chile. We show two seasons and  
 347 months to examine possible differences between the dry and wet seasons. Additionally,  
 348 the results from different GCMs are stratified according to their historical raw perfor-  
 349 mance, measured by the Taylor Skill Score. As in Figure 4, the ANOVA analysis for his-  
 350 torical biases shows differences among temporal stratifications, especially when compared  
 351 to annual biases (Figure 5a). Because the relative contributions of BCM and TS to pre-  
 352 precipitation biases do not greatly differ among climate groups, we show results at the na-  
 353 tional scale. The choice of BCM explains most of the variance for the mean annual pre-  
 354 cipitation bias, whereas the choice of TS explains almost all the variance for mean sea-  
 355 sonal and monthly precipitation biases. It is worth noting that the biases at the annual  
 356 scale are, in general, very low (Figure 4, <1%), and that the relative importance of the  
 357 choice of TS for seasonal and monthly biases does not decrease for GCMs with high TSS  
 358 values. The latter result is counterintuitive since one might expect that GCMs with good  
 359 raw precipitation seasonality will be effectively bias-corrected, regardless of the TS se-  
 360 lected. For variables related to quantiles (highest 1% daily precipitation, dry and wet-

spell lengths, and wet-day fraction), the relative importance of BCMs increases for GCMs with higher TSS, being BCM the most important decision, even at seasonally and monthly time scales (Figure S1).

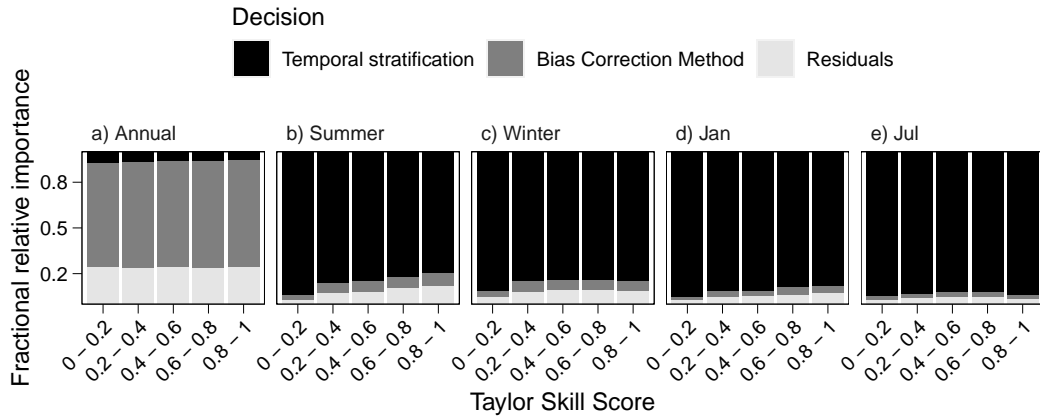


**Figure 5.** Relative importance (as a fraction averaged from all grid cells and GCMs for continental Chile) of the bias correction method and the temporal stratification to explain the precipitation biases at the annual, seasonal (DJF and JJA), and monthly (January and July) time scales during the historical period (1980-2014), for different levels of historical GCM performance (x-axis). Biases are computed after applying BCMs.

#### 4.3 Projected changes

We now analyze the interplay between the choice of TS, the raw GCM precipitation seasonality, and its effects on projected changes in precipitation for the period 2065-2099 (with respect to 1980-2014) at different time scales. Figure 6 displays projected changes in mean annual, seasonal, and monthly precipitation for one grid cell located in central Chile (red dot in map) and one GCM (INM-CM4-8) with a high  $R$  value. For this GCM and grid cell,  $TSS = 0.76$  during the period 1980-2014, with a Pearson correlation coefficient between mean monthly raw GCM and reference amounts of 0.98, and a 41% underestimation of the standard deviation. The high value of  $R$  indicates a good seasonality of raw GCM outputs. Figure 6 shows that different BCMs yield a high dispersion in projected changes of mean annual precipitation (different lines), with little influence on the selected TS (x-axis of each subplot). Additionally, all BCMs alter the raw GCM projection. For example, if all BCMs are applied using the entire dataset, projected changes in summer precipitation range between -8% to 5%, whereas the raw projection is close to -30%. The application of MBCn using the entire period yields a positive projected change in the mean summer precipitation, while a seasonal and monthly application of the same BCM projects a decrease in summer precipitation. The results for individual months (January and July) reveal more dispersion and interaction among BCMs and the choice of TS. For example, applying the BCM with the entire time series results in positive and negative projections of mean July precipitation (the雨iest month for this grid cell). Similarly, different TSs can also provide different projected signals.

Figure 6 reveals that the choice of TS affects the signal of projected changes in summer precipitation (e.g., for the MBCn method) and, in particular, in January and July precipitation amounts. The TS can be considered relevant for a specific grid cell if it is able to switch the projected signal of a variable for a particular GCM-BCM combination. This is, for example, the case of mean July precipitation (Figure 6), for which the

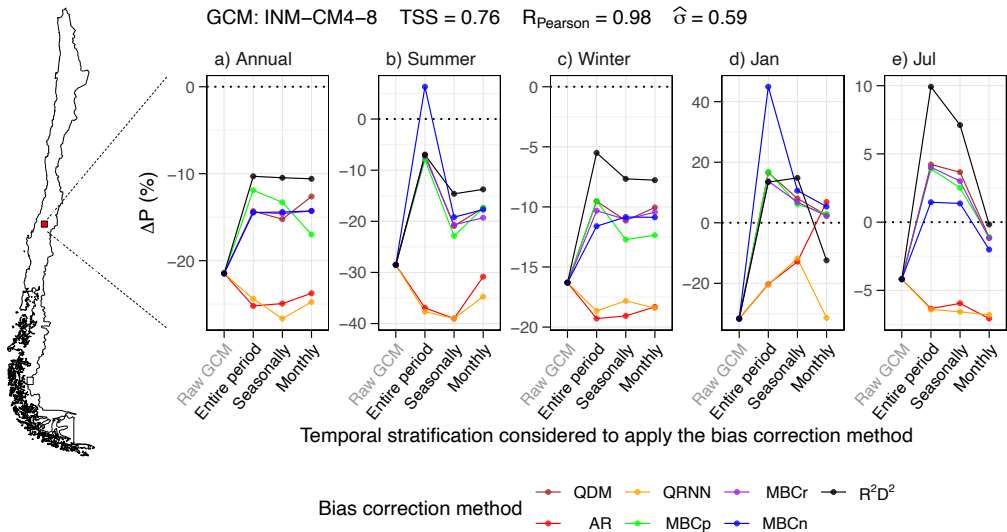


**Figure 6.** Projected change in annual, seasonal (summer and winter), and monthly (January and July) precipitation for different temporal stratifications (x-axis) and bias correction methods (lines). All combinations of TS and BCM decisions, along with projected changes from the raw (biased) GCMs, are displayed. The results are valid only for the grid cell shown and the GCM INM-CM4-8. The metrics (e.g., TSS) were computed using the raw (biased) GCM data for the period 1980-2014.

signal of projected changes is different among TSs for the MBCn, MBCr, and  $R^2D^2$  methods.

Figure 7 shows, for all the grid cells analyzed, the fraction of ‘well-behaved’ GCMs (i.e., with  $TSS \geq 0.7$ ; e.g., Kwon et al., 2019) for which the selection of TS leads to different signs in projected precipitation changes. Note that the number of GCMs that meet the performance requirement - obtained by spatially averaging the number of GCMs with  $TSS \geq 0.7$  at each latitudinal band - varies along the domain. In general, the choice of TS does not alter the signal of projected changes in mean annual precipitation, although a few GCMs are affected by this decision in some areas (e.g., northern Chile). Nevertheless, the effects of TS are more evident in seasonal projections (Figure 7b and 7c). During the summer, >50% of the number of GCMs are affected by the TS in Central Chile (dry season). During winter, the Altiplano region and part of southern Chile are largely influenced by the choice of TS. It should be noted, however, that the summer season in Central Chile and the winter season in the Altiplano region are dry seasons. Therefore, while the signal of projected changes may vary for different TSs, the precipitation amounts involved are small. For mean monthly January and July precipitation, the choice of TS is even more relevant. Indeed, nearly all GCMs are affected by the TS along the coast of northern Chile, while ~50% of the GCMs yield different signals in projected changes for different TSs in Central Chile. The case of July is more interesting since it is the rainiest month in most of continental Chile. In July, ~50% of the GCMs are affected by the TS along the Central Chilean Andes (western border), impacting the accumulation of snow and, therefore, meltwater volume and timing estimates for the spring and summer seasons. In southern Chile, one can find grid cells where GCMs are affected by the TS decision, though that fraction is lower compared to the Central Chilean Andes.

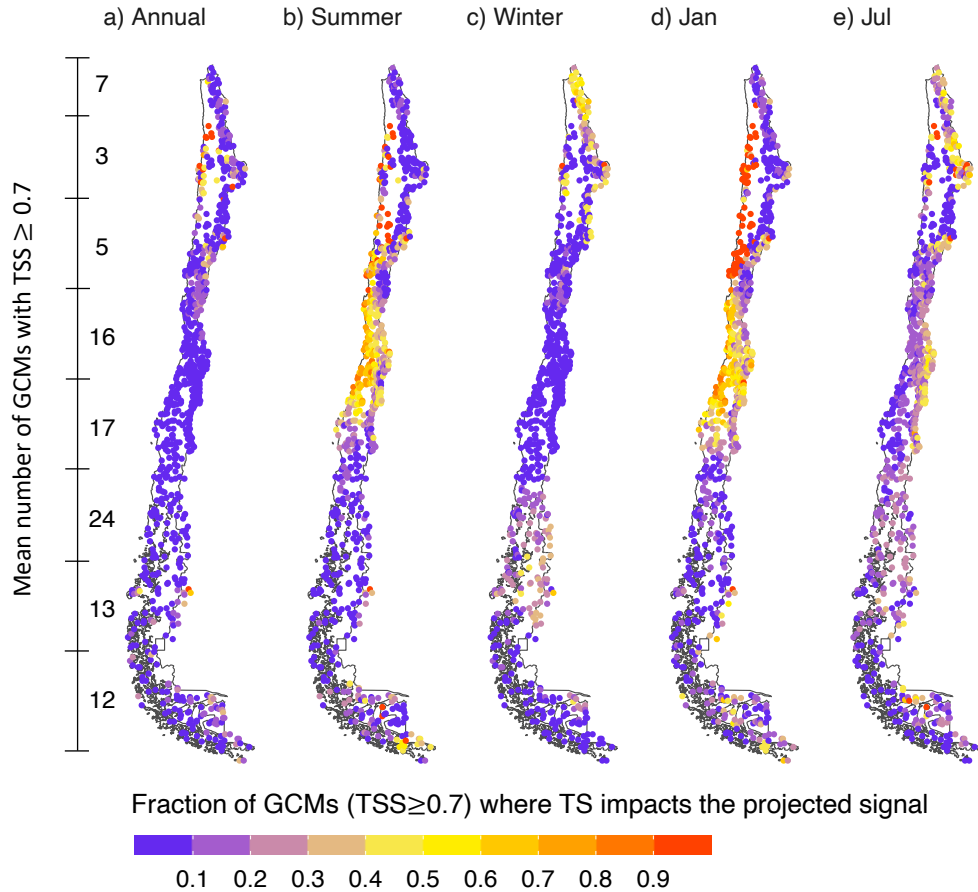


**Figure 7.** Fraction of GCMs with acceptable performance (i.e., with  $TSS \geq 0.7$ ) for which the TS yields different projected precipitation signals. The number of GCMs that meet the threshold criteria at each  $\sim 5^\circ$  latitudinal band is computed as the average of GCMs with  $TSS \geq 0.7$  from all grid cells within that band.

Figure 8a compares the raw GCM output (obtained from the GCM ACCESS-CM2) and the reference precipitation seasonality over a historical period at one grid cell located in central-southern Chile (red dot on the map). For this GCM-grid cell combination,  $TSS = 0.96$ ,  $R = 0.94$  and  $\hat{\sigma} = 1.08$ . Note that the GCM simulates the maximum monthly precipitation in July instead of June (when the maximum occurs according to the reference). Figure 8b displays, for the same GCM-grid cell, the projected precipitation seasonality for each BCM-TS combination (thin lighter lines). The results show that applying a BCM using the entire period (green lines) provides the same seasonality as the raw GCM; however, seasonal and monthly TSs distort the raw projected seasonality. Further, when BCMS are applied using a monthly TS (black/gray lines), the projected month of maximum precipitation is June, whereas for seasonal and entire period such month is July. Additionally, seasonal and monthly TSs yield higher precipitation fractions (compared to the raw GCM) during April and May, and smaller values during September and October. Such differences in projected precipitation seasonality may affect any subsequent analyses of simulated hydrological fluxes and states.

To examine the extent to which projected precipitation seasonality is affected by the temporal stratification, we focus on the projected maximum mean monthly precipitation. Hence, we contrast, for each GCM-grid cell combination, three curves obtained with the three temporal stratifications (each obtained by averaging the projections among BCMS for each GCM). We consider that the TS affects the projected seasonality if the month where the maximum mean monthly precipitation amount occurs differs. Conversely, if such a month is the same for the three TSs, we consider that this decision does not impact the seasonality. Figure 8c displays the fraction of the number of GCMs with  $TSS \geq 0.7$  for which the TS impacts the projected precipitation seasonality. Interestingly, the number is relatively high (>40%) for most of continental Chile. The fraction of GCMs affected by the TS decision is even higher in northern Chile, the Central Chilean Andes, and the Southernmost part of Chile, where more than 60% of GCMs are affected.

## 5 Discussion

The results presented here highlight the relevance of the temporal stratification used when applying bias correction techniques, which affects (i) SDBC-biases in seasonal and monthly precipitation amounts over a historical period, and (ii) the signal of projected changes and the seasonality of projections.

### 5.1 Temporal stratification as a source of uncertainty

Our results show that the temporal stratification can largely affect precipitation biases during a historical period, as well as the signal and seasonality of projected changes. However, this methodological choice has been rarely explored in climate change impact assessments, and the lack of guidance has motivated the use of more than one TS in some studies (e.g., Wootten et al., 2021). Further, model errors may not necessarily be removed in the process. For example, Hakala et al. (2018) obtained that biases in precipitation and streamflow seasonality remained after applying BCMS. Here, we found that only a monthly application of the BCM can replicate the reference precipitation seasonality, even for GCMs with a good raw representation of annual cycles.

### 5.2 Projected seasonality

Our study reveals that one of the main effects of selecting different TSs is the possibility to distort the precipitation seasonality projected by raw GCM outputs. In hydrologic impact assessments, this artifact may propagate into the timing of simulated variables like snow accumulation and melting, energy fluxes, and streamflow (Meyer et al., 2019). Our results show that when the raw GCM seasonality has timing errors (com-

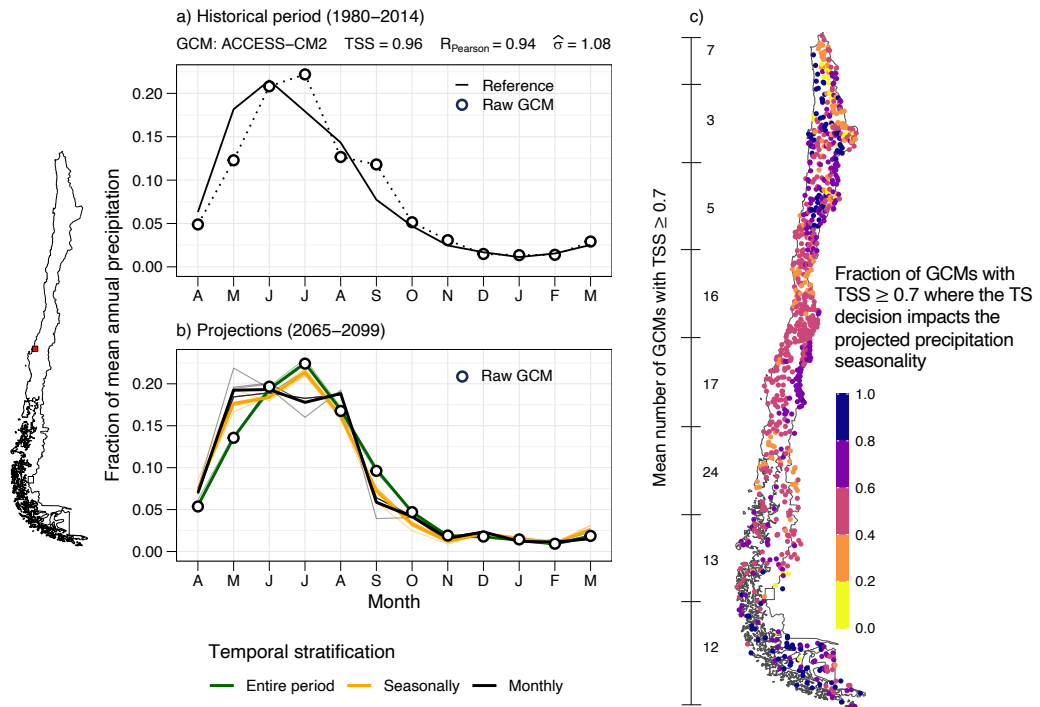


**Figure 8.** Influence of the temporal stratification used to apply bias correction methods on the projected precipitation seasonality. (a) Dimensionless historical seasonality for one grid cell (red dot on the map) and one GCM (ACCESS-CM2). Note that the sum of monthly fractions is equal to 1. (b) Projected raw (circles) and bias-corrected (colored lines) GCM precipitation seasonality. Lighter and thinner lines represent different BCMs, whereas thick lines represent the average across BCMs. (c) Fraction of the total number GCMs with  $TSS \geq 0.7$ , for which the temporal stratification yields different projected seasonality, measured as different months for maximum mean monthly precipitation for the 2065–2099 period. In c), the average number of GCMs meeting the TSS criterion is computed for latitudinal bands.

pared to the reference), a pronounced shift in the projected seasonality can be obtained after applying BCMs (compared to the case without bias correction). However, when the raw GCM replicates the historically observed precipitation seasonality reasonably well, one might expect that different TSs yield the same projected seasonality. To test this hypothesis, we compare the precipitation seasonality projected with three TSs (bottom panels) by two GCMs (CanESM5 and NorESM2-MM, Figure 9) that replicate annual cycles (i.e., high Pearson correlation coefficients, with GCM and reference maximum mean monthly precipitation being the same, top panels). For GCM CanESM5 (Figure 9a), the choice of TS has little effect on the projected precipitation seasonality. Conversely, the temporal stratification affects the seasonality projected by NorESM2 (Figure 9b). For example, if the BCM is applied seasonally and monthly, the months of maximum mean monthly precipitation are May and August, respectively. Interestingly,  $TSS = 0.951$  for this GCM, which is higher than the value obtained for CanESM5 (0.694), and both GCMs have similar Pearson correlation coefficients. These results emphasize that even GCMs with a good raw representation of historical seasonality can be affected by the temporal stratification used to apply BCMs.

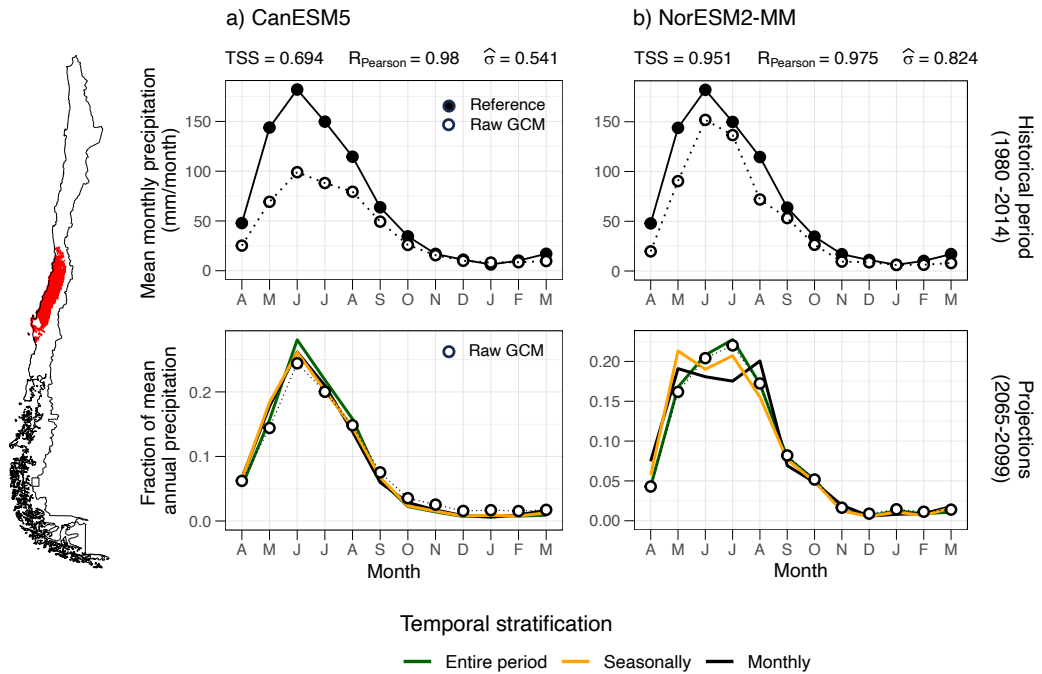


**Figure 9.** Impact of the temporal stratification used in bias correction for two GCMs. The results presented here are spatially averaged values of the grid cells contained in climate group 6 (highlighted in red on the map). Top row: comparison of the raw GCMs and the reference for the period 1980-2014. Bottom row: projected precipitation seasonality in terms of fraction of mean annual precipitation (average from the seven BCMS).

### 5.3 A priori evaluation of the TS impact on projected precipitation seasonality

Understanding the potential effects of the TS on the projected signal and seasonality of precipitation from a specific GCM could be helpful for a more detailed assess-

ment of climate change and/or hydrological changes. Here, we propose using the linear scaling method (LSM) (Widmann et al., 2003; Maraun, 2016) - due to its low computational cost and simplicity (Lafon et al., 2013; Chaubey & Mall, 2023) -, as a quick diagnostics tool to inform if the TS may be an influential decision (an example of an LSM application is provided in Appendix B). The LSM removes the bias from the raw GCM time series ( $f_{bias}$ ) through a multiplicative factor for the case of precipitation and an additive term for temperature, using an observational dataset as a reference. For example, if the reference and raw GCM mean annual precipitation amounts are 500 mm/year and 650 mm/year, respectively, a factor  $f_{bias} = 500/650 = 0.77$  is applied to the raw GCM time series to remove the bias. Accordingly, seasonal or monthly applications of LSM require more scaling factors (Maraun et al., 2010). Hence, the raw GCM projected change ( $f_\Delta$ ) is preserved (at the TS time scale), since the scaling factors are typically considered to be time-invariant. Additionally, the influence of the temporal stratification and the reference dataset (in case there is more than one available) can be isolated for a specific grid cell-GCM combination.

Figure 10a illustrates the application of the linear scaling method (dashed lines) to the GFDL-CM4 GCM in one grid cell (red dot in map), using the entire period and stratifying the data seasonally and monthly. For this GCM-grid cell combination,  $TSS = 0.72$  and  $R = 0.7$ , and different TSSs yield different projected precipitation seasonalities when applying the LSM. Figure 10a shows that the precipitation factors obtained with LSM agree with the averages obtained from all (seven) bias correction methods (solid lines).

Finally, we examine the capability of the LSM to identify the precipitation seasonality projected with different TSs correctly. To this end we obtain, for each grid cell-GCM-TS combination, the precipitation seasonalities from (i) the average between the seven BCMs, and (ii) the application of the LSM. If the months of the projected maximum precipitation agree, we consider that the LSM correctly identifies the seasonality, and if this occurs for the three TSs, we consider that the LSM successfully identifies the projected bias-corrected seasonality for that specific grid cell-GCM combination. Figure 10a illustrates a successful case since, for each TS, the month of maximum precipitation is the same for the average among seven BCMs and from the LSM. Then we compute, for the 1,000 grid cells analyzed here, the fraction of GCMs for which the LSM successfully identifies the projected seasonality (accuracy, Figure 10b). The results show that, in almost all the grid cells, the LSM successfully identifies the projected seasonality of  $\sim 70\%$  of the GCMs, whereas for most grid cells ( $> 85\%$ ), the LSM successfully projects the seasonality for more than 85% of the GCMs.

#### 5.4 Limitations and future work

In this study, we selected the SSP5-8.5 scenario and 29 GCMs, although other future scenarios and/or a subset of GCMs could be considered to assess the effects on historical biases (after bias correction) and/or future projections. We did not focus on performance metrics for specific GCMs because evaluating the adequacy of particular bias correction methods is out of the scope of this work; instead, we focus on how these techniques are traditionally applied. Although we selected univariate and multivariate BCMs (e.g., Q. Guo et al., 2020), quantile-based, neural networks, and linear regressions, different approaches could be considered.

Additionally, we did not conduct any hydrological modeling. Instead, we focused on the repercussions of some decisions on the historical biases and the projected seasonality of climate variables required to run hydrological and land surface models. However, previous work has shown that hydrological models tend to amplify biases in the forcings (Teng et al., 2015). We emphasize that any assessment of climate change impacts should ensure that the climatological annual cycles of hydrological simulations forced with (i)

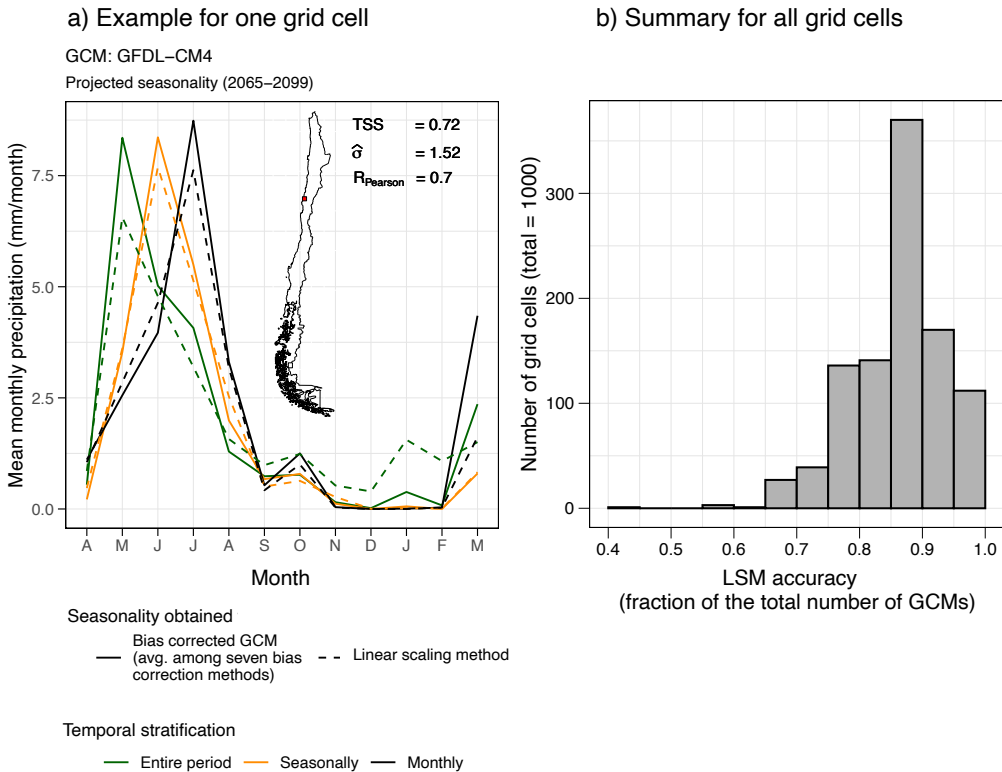


**Figure 10.** Linear scaling method used as a proxy to estimate the projected precipitation seasonality. (a) Example of projected precipitation seasonalities for one grid cell and one GCM, obtained from applying the LSM and the seven BCMs tested. The metrics summarize the raw (biased) GCM performance for the historical period (1980–2014). (b) LSM accuracy (as a fraction of the total number of GCMs) for all grid cells.

reference data sets and (ii) bias-corrected time series from GCMs/RCMs are similar (Hakala et al., 2018). Hence, verifying the reference and bias-corrected GCM forcing data during a historical period arises as a crucial step (Chen et al., 2013; Clark et al., 2016; Mendoza et al., 2016; Melsen et al., 2019). Future work could consider the impacts of SDBC historical biases and differences in projected seasonality on different aspects of the hydrograph (e.g., mean values, extremes, timing, etc.) and signatures formulated from other variables than streamflow (e.g., SWE, soil moisture; McMillan et al., 2022; Araki et al., 2022).

## 6 Conclusions

In this paper, we examined how methodological choices involved in GCM bias correction affect historical and future climate portrayals. To this end, we used seven bias correction methods, 29 CMIP6 GCMs, and three temporal stratifications. All the configurations were applied to daily time series of precipitation and maximum and minimum daily temperature derived from the CR2MET gridded observational product, available for continental Chile. Our main findings are as follows:

1. A monthly application of bias correction methods is required to replicate the reference precipitation seasonality, even for GCMs with good raw seasonality.
2. The temporal stratification is the most relevant decision to quantify seasonal and monthly precipitation biases.
3. Different temporal stratifications may yield different projected signals and seasonality, even for GCMs with good raw seasonality.
4. The linear scaling method can be used to estimate the projected seasonality of GCMs and, therefore, to identify the climate models for which the choice of temporal stratification may be critical, before applying more sophisticated and computationally expensive bias correction methods.

## Appendix A Selected GCMs

Table A1 shows the GCMs included in this study.

## Appendix B Scaling factor example

We illustrate the effects of the temporal stratification by applying the linear scaling method (LSM) (Maraun et al., 2010) for one grid cell-GCM combination. Figure B1a shows monthly precipitation averages from raw GCM outputs, whereas Figure B1b-d shows the bias-corrected GCM values for three different temporal stratifications. Monthly values were obtained from the daily corrected time series.

Note that when the entire period is used to bias-correct the GCM, only one factor is applied. In the grid cell analyzed, the reference annual precipitation is 4371 mm, which is below the historical raw GCM amount for the same period (5020 mm). Hence, the raw GCM precipitation time series is multiplied by the factor  $f = 4731/5020 = 0.87$ , which removes the annual SDBC bias; nevertheless, monthly SDBC-biases persist (see differences between black and blue lines in Figure B1b). When the LSM is applied seasonally, four factors are used to multiply the raw GCM time series. For example, daily values from March, April, and May are bias-corrected by the seasonal factor obtained from the reference (1134 mm/season) and the raw GCM (1498 mm/season) precipitation amounts. In this case, the factor used to bias-correct daily precipitation from March, April, and May is  $f_{MAM} = 1134/1498 = 0.76$ . Similarly, if the LSM is applied monthly, daily precipitation amounts from March are bias-corrected using the reference (374 mm/month) and raw GCM (498 mm/month), which yields a factor  $f = 374/498 = 0.75$ . For the monthly TS, the black and blue lines are the same. Note that the projected maximum

**Table A1.** GCMs considered in this study

GCM	$\Delta\text{lat}$	$\Delta\text{lon}$	Institution
ACCESS-CM2	1.25	1.88	Australian Research Council Centre of Excellence for Climate Science, Australia.
ACCESS-ESM1-5	1.25	1.88	
BCC-CSM2-MR	1.11	1.13	Beijing Climate Center, China.
CanESM5	2.77	2.81	Canadian Centre for Climate Modelling and Analysis, Canada.
CMCC-ESM2	0.94	1.25	Euro-Mediterranean Centre on Climate Change Coupled Climate Model, Italy.
CNRM-CM6-1-HR	0.50	0.50	
CNRM-CM6-1	1.40	1.40	Centre National de Recherches Météorologiques (CNRM), France.
CNRM-ESM2-1	1.40	1.41	
E3SM-1-0	1.00	1.00	Lawrence Livermore National Laboratory, USA.
EC-Earth3-CC	0.70	0.70	
EC-Earth3-Veg-LR	1.12	1.13	EC-Earth Consortium, Europe.
EC-Earth3-Veg	0.70	0.70	
EC-Earth3	0.70	0.70	
FGOALS-g3	2.18	2.00	Chinese Academy of Sciences Flexible Global Ocean-Atmosphere-Land System Model, China.
GFDL-CM4	1.00	1.25	
GFDL-ESM4	1.00	1.25	Geophysical Fluid Dynamics Laboratory, USA.
INM-CM4-8	1.50	2.00	
INM-CM5-0	1.50	2.00	Institute for Numerical Mathematics, Russia.
IPSL-CM6A-LR	1.27	2.50	Institute Pierre Simon Laplace (IPSL), France.
KACE-1-0-G	1.25	1.88	National Institute of Meteorological Sciences (NIMS) and Korea Meteorological Administration (KMA), South Korea.
KIOST-ESM	1.88	1.88	Korea Institute of Ocean Science and Technology Earth System Model and Its Simulation Characteristics, South Korea.
MIROC-ES2L	2.79	2.81	
MIROC6	1.39	1.41	Japan Agency for Marine-Earth Science and Technology (JAMSTEC), Japan.
MPI-ESM1-2-HR	0.93	0.94	
MPI-ESM1-2-LR	1.87	1.88	Max Planck Institute for Meteorology (MPI-M), Germany.
MRI-ESM2-0	1.11	1.13	Meteorological Research Institute, Japan.
NESM3	1.85	1.88	Nanjing University of Information Science and Technology Earth System Model, China.
NorESM2-MM	0.94	1.25	NorESM Climate modeling Consortium, Oslo, Norway.
TaiESM1	0.94	1.25	Research Center for Environmental Changes, Academia Sinica, Nankang, Taipei, Taiwan.

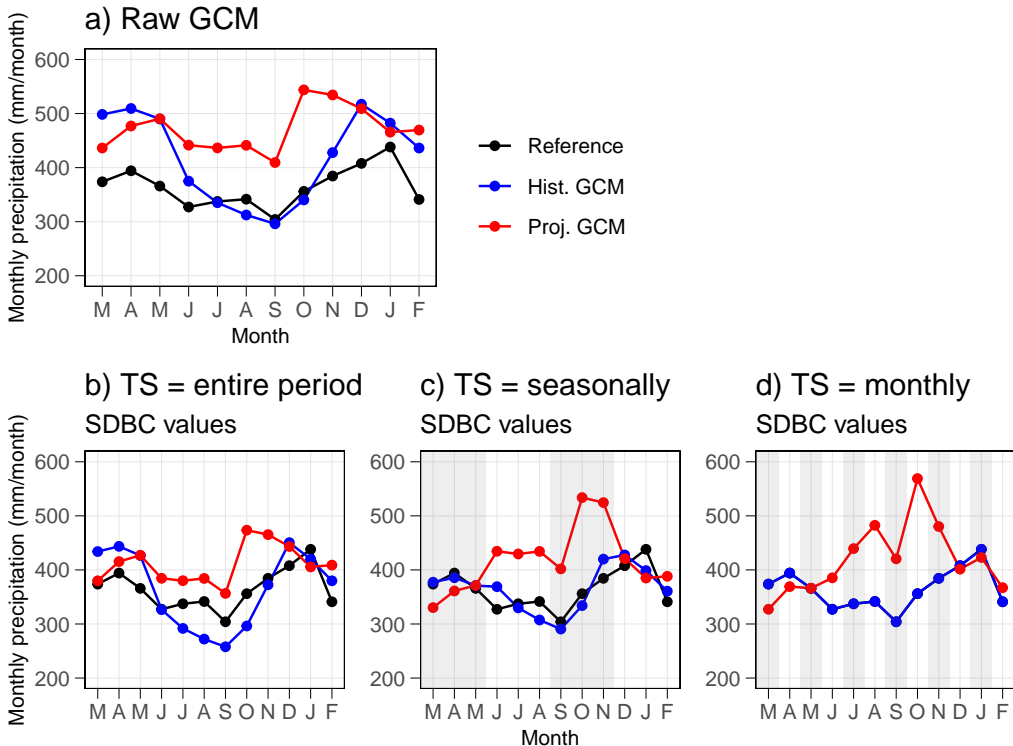


**Figure B1.** Illustration of the linear scaling method, applied to one grid cell-GCM combination, and its effects on the SDBC-biases and projections. (a) Reference (observational) and raw GCM seasonality during the period 1980–2014 (black and blue lines). The projected raw seasonality is also shown in red (2065–2099). (b), (c) and (d) show the bias-corrected precipitation amounts using the entire period, seasons, and months, respectively, for temporal stratification. The reference value is shown in all panels for completeness, and the shaded areas represent the temporal stratification.

monthly precipitation is October for the three TS, which is the same as the raw GCM projection. However, the projected minimum monthly precipitation is September, March, and March for the entire period, season, and monthly application of the LSM, respectively.

## Open Research Section

The CR2MET dataset (Boisier et al., 2018) is available at <https://www.cr2.cl/datos-productos-grillados/>. The GCMs data was downloaded from the Earth System Grid Federation (<https://esgf-node.llnl.gov/search/cmip6/>). All the data used in this study is available at <https://bhuch.myqnapcloud.com/share.cgi?ssid=43cb3da649cd41ca9bfc42150a855e89>.

## Acknowledgments

Nicolás Vásquez and Pablo A. Mendoza received support from the Fondecyt project No. 11200142. Nicolás Vásquez also received support from the Emerging Leaders in the Americas Program (ELAP) scholarship (Canada) and the ANID Doctorado Nacional schol-

593 arship No. 21230289 (Chile). Pablo A. Mendoza was also supported by ANID/PIA project  
 594 No. AFB230001.

## 595 References

- 596 Aceituno, P., Boisier, J. P., Garreaud, R., Rondanelli, R., & Rutllant, J. A. (2021).  
 597 Climate and Weather in Chile. In *Water resources of chile* (pp. 7–29). doi: 10  
 598 .1007/978-3-030-56901-3{\\_}2
- 599 Addor, N., Rössler, O., Köplin, N., Huss, M., Weingartner, R., & Seibert, J.  
 600 (2014). Robust changes and sources of uncertainty in the projected hy-  
 601 drological regimes of Swiss catchments. *Water Resources Research*. doi:  
 602 10.1002/2014WR015549
- 603 Alder, J. R., & Hostetler, S. W. (2019). The Dependence of Hydroclimate Projec-  
 604 tions in Snow-Dominated Regions of the Western United States on the Choice  
 605 of Statistically Downscaled Climate Data. *Water Resources Research*. doi:  
 606 10.1029/2018WR023458
- 607 Araki, R., Branger, F., Wiekenkamp, I., & McMillan, H. (2022, 4). A signature-  
 608 based approach to quantify soil moisture dynamics under contrasting land-  
 609 uses. *Hydrological Processes*, 36(4). doi: 10.1002/hyp.14553
- 610 Boisier, J. P., Álvarez-Garretón, C., Cepeda, J., Osses, A., Vásquez, N., & Ron-  
 611 danelli, R. (2018). CR2MET: A high-resolution precipitation and temperature  
 612 dataset for hydroclimatic research in Chile. In *Egu general assembly conference  
 613 abstracts* (p. 19739).
- 614 Cannon, A. J. (2011, 9). Quantile regression neural networks: Implementation in  
 615 R and application to precipitation downscaling. *Computers & Geosciences*,  
 616 37(9), 1277–1284. doi: 10.1016/j.cageo.2010.07.005
- 617 Cannon, A. J. (2016, 10). Multivariate Bias Correction of Climate Model Output:  
 618 Matching Marginal Distributions and Intervariable Dependence Structure.  
 619 *Journal of Climate*, 29(19), 7045–7064. doi: 10.1175/JCLI-D-15-0679.1
- 620 Cannon, A. J. (2018). Multivariate quantile mapping bias correction: an  
 621 N-dimensional probability density function transform for climate model  
 622 simulations of multiple variables. *Climate Dynamics*. doi: 10.1007/  
 623 s00382-017-3580-6
- 624 Cannon, A. J., Sobie, S. R., & Murdock, T. Q. (2015). Bias correction of GCM  
 625 precipitation by quantile mapping: How well do methods preserve changes in  
 626 quantiles and extremes? *Journal of Climate*. doi: 10.1175/JCLI-D-14-00754.1
- 627 Chaubey, P. K., & Mall, R. K. (2023, 9). Intensification of Extreme Rainfall in In-  
 628 dian River Basin: Using Bias Corrected CMIP6 Climate Data. *Earth's Future*,  
 629 11(9). doi: 10.1029/2023EF003556
- 630 Cheeseman, P., John, R., & Nasa, S. (1996). Bayesian Classification (AutoClass):  
 631 Theory and Results. *Advances in knowledge discovery and data mining*.
- 632 Cheeseman, P., Kelly, J., Self, M., Stutz, J., Taylor, W., & Freeman, D. (1988, 1).  
 633 AutoClass: A Bayesian Classification System. *Machine Learning Proceedings  
 634 1988*, 54–64. doi: 10.1016/B978-0-934613-64-4.50011-6
- 635 Chegwidden, O. S., Nijssen, B., Rupp, D. E., Arnold, J. R., Clark, M. P., Hamman,  
 636 J. J., ... Xiao, M. (2019). How Do Modeling Decisions Affect the Spread  
 637 Among Hydrologic Climate Change Projections? Exploring a Large Ensem-  
 638 ble of Simulations Across a Diversity of Hydroclimates. *Earth's Future*. doi:  
 639 10.1029/2018EF001047
- 640 Chen, J., Arseneault, R., Brissette, F. P., & Zhang, S. (2021). Climate Change  
 641 Impact Studies: Should We Bias Correct Climate Model Outputs or  
 642 Post-Process Impact Model Outputs? *Water Resources Research*. doi:  
 643 10.1029/2020WR028638
- 644 Chen, J., Brissette, F. P., Chaumont, D., & Braun, M. (2013, 7). Finding appropri-  
 645 ate bias correction methods in downscaling precipitation for hydrologic impact

- 646 studies over North America. *Water Resources Research*, 49(7), 4187–4205. doi:  
 647 10.1002/wrcr.20331
- 648 Clark, M. P., Wilby, R. L., Gutmann, E. D., Vano, J. A., Gangopadhyay, S., Wood,  
 649 A. W., ... Brekke, L. D. (2016, 6). Characterizing Uncertainty of the Hy-  
 650 drologic Impacts of Climate Change. *Current Climate Change Reports*, 2(2),  
 651 55–64. doi: 10.1007/s40641-016-0034-x
- 652 Coron, L., Thirel, G., Delaigue, O., Perrin, C., & Andréassian, V. (2017, 8). The  
 653 suite of lumped GR hydrological models in an R package. *Environmental Mod-  
 654 elling & Software*, 94, 166–171. doi: 10.1016/j.envsoft.2017.05.002
- 655 Dettinger, Cayan, D., Meyer, M., & Jeton, A. (2004). Simulated Hydrologic Re-  
 656 sponds To Climate Variations. *Climatic Change*.
- 657 DGA. (2022). *Homologación del cálculo hidrológico para la estimación de la oferta*  
 658 *natural del agua histórica y futura en Chile*. (Tech. Rep.). SIT N° 524. Min-  
 659 isterio de Obras Públicas, Dirección General de Aguas, División de Estudios  
 660 y Planificación, Chile. Elaborado por Universidad de Chile, Facultad de Cien-  
 661 cias Físicas y Matemáticas. Retrieved from <https://snia.mop.gob.cl/repositoriodga/handle/20.500.13000/126394>
- 662 Di Virgilio, G., Ji, F., Tam, E., Nishant, N., Evans, J. P., Thomas, C., ... Delage,  
 663 F. (2022, 4). Selecting CMIP6 GCMs for CORDEX Dynamical Downscal-  
 664 ing: Model Performance, Independence, and Climate Change Signals. *Earth's*  
 665 *Future*, 10(4). doi: 10.1029/2021EF002625
- 666 François, B., Vrac, M., Cannon, A. J., Robin, Y., & Allard, D. (2020, 6). Multi-  
 667 variate bias corrections of climate simulations: which benefits for which losses?  
 668 *Earth System Dynamics*, 11(2), 537–562. doi: 10.5194/esd-11-537-2020
- 669 Ghimire, U., Srinivasan, G., & Agarwal, A. (2019, 3). Assessment of rainfall bias  
 670 correction techniques for improved hydrological simulation. *International Jour-  
 671 nal of Climatology*, 39(4), 2386–2399. doi: 10.1002/joc.5959
- 672 Guo, J., Wang, X., Fan, Y., Liang, X., Jia, H., & Liu, L. (2023, 4). How Ex-  
 673 treme Events in China Would Be Affected by Global Warming—Insights  
 674 From a Bias-Corrected CMIP6 Ensemble. *Earth's Future*, 11(4). doi:  
 675 10.1029/2022EF003347
- 676 Guo, Q., Chen, J., Zhang, X. J., Xu, C., & Chen, H. (2020, 5). Impacts of Us-  
 677 ing State-of-the-Art Multivariate Bias Correction Methods on Hydrologi-  
 678 cal Modeling Over North America. *Water Resources Research*, 56(5). doi:  
 679 10.1029/2019WR026659
- 680 Gutiérrez, J. M., Maraun, D., Widmann, M., Huth, R., Hertig, E., Benestad, R.,  
 681 ... Pagé, C. (2019, 7). An intercomparison of a large ensemble of statistical  
 682 downscaling methods over Europe: Results from the VALUE perfect predic-  
 683 tor cross-validation experiment. *International Journal of Climatology*, 39(9),  
 684 3750–3785. doi: 10.1002/joc.5462
- 685 Gutmann, E., Pruitt, T., Clark, M. P., Brekke, L., Arnold, J. R., Raff, D. A., &  
 686 Rasmussen, R. M. (2014). An intercomparison of statistical downscaling meth-  
 687 ods used for water resource assessments in the United States. *Water Resources*  
 688 *Research*. doi: 10.1002/2014WR015559
- 689 Haerter, J. O., Hagemann, S., Moseley, C., & Piani, C. (2011, 3). Climate model  
 690 bias correction and the role of timescales. *Hydrology and Earth System Sci-  
 691 ences*, 15(3), 1065–1079. doi: 10.5194/hess-15-1065-2011
- 692 Hagemann, S., Chen, C., Haerter, J. O., Heinke, J., Gerten, D., & Piani, C. (2011,  
 693 8). Impact of a Statistical Bias Correction on the Projected Hydrological  
 694 Changes Obtained from Three GCMs and Two Hydrology Models. *Journal of*  
 695 *Hydrometeorology*, 12(4), 556–578. doi: 10.1175/2011JHM1336.1
- 696 Hakala, K., Addor, N., & Seibert, J. (2018, 8). Hydrological Modeling to Evaluate  
 697 Climate Model Simulations and Their Bias Correction. *Journal of Hydrometeo-  
 698 rology*, 19(8), 1321–1337. doi: 10.1175/JHM-D-17-0189.1
- 699 Han, P., Long, D., Han, Z., Du, M., Dai, L., & Hao, X. (2019, 4). Improved un-

- derstanding of snowmelt runoff from the headwaters of China's Yangtze River  
701 using remotely sensed snow products and hydrological modeling. *Remote*  
702 *Sensing of Environment*, 224, 44–59. doi: 10.1016/j.rse.2019.01.041
- Hanus, S., Hrachowitz, M., Zekollari, H., Schoups, G., Vizcaino, M., & Kaitna, R.  
703 (2021). Future changes in annual, seasonal and monthly runoff signatures  
704 in contrasting Alpine catchments in Austria. *Hydrology and Earth System*  
705 *Sciences*. doi: 10.5194/hess-25-3429-2021
- Hattermann, F. F., Vetter, T., Breuer, L., Su, B., Daggupati, P., Donnelly, C., ...  
706 Krysnaova, V. (2018). Sources of uncertainty in hydrological climate im-  
707 pact assessment: A cross-scale study. *Environmental Research Letters*. doi:  
708 10.1088/1748-9326/aa9938
- Her, Y., Yoo, S. H., Cho, J., Hwang, S., Jeong, J., & Seong, C. (2019). Uncertainty  
712 in hydrological analysis of climate change: multi-parameter vs. multi-GCM  
713 ensemble predictions. *Scientific Reports*. doi: 10.1038/s41598-019-41334-7
- Hersbach, H., Bell, B., Berrisford, P., Hirahara, S., Horányi, A., Muñoz-Sabater, J.,  
715 ... Thépaut, J. (2020, 7). The ERA5 global reanalysis. *Quarterly Journal of*  
716 *the Royal Meteorological Society*, 146(730), 1999–2049. doi: 10.1002/qj.3803
- Hess, P., Lange, S., Schötz, C., & Boers, N. (2023, 10). Deep Learning for Bias-  
718 Correcting CMIP6-Class Earth System Models. *Earth's Future*, 11(10). doi:  
719 10.1029/2023EF004002
- Jennings, K. S., Winchell, T. S., Livneh, B., & Molotch, N. P. (2018, 3). Spatial  
722 variation of the rain–snow temperature threshold across the Northern Hemis-  
723 phere. *Nature Communications*, 9(1), 1148. doi: 10.1038/s41467-018-03629-7
- Knoben, W. J., Woods, R. A., & Freer, J. E. (2018). A Quantitative Hydrologi-  
724 cal Climate Classification Evaluated With Independent Streamflow Data. *Wa-  
725 ter Resources Research*. doi: 10.1029/2018WR022913
- Kwon, S., Kim, J., Boo, K., Shim, S., Kim, Y., & Byun, Y. (2019, 3). Performance-  
727 based projection of the climate-change effects on precipitation extremes in  
728 East Asia using two metrics. *International Journal of Climatology*, 39(4),  
729 2324–2335. doi: 10.1002/joc.5954
- Lafon, T., Dadson, S., Buys, G., & Prudhomme, C. (2013, 5). Bias correction  
732 of daily precipitation simulated by a regional climate model: a comparison  
733 of methods. *International Journal of Climatology*, 33(6), 1367–1381. doi:  
734 10.1002/joc.3518
- Maraun, D. (2016, 12). Bias Correcting Climate Change Simulations - a Critical Re-  
735 view. *Current Climate Change Reports*, 2(4), 211–220. doi: 10.1007/s40641  
736 -016-0050-x
- Maraun, D., Wetterhall, F., Ireson, A. M., Chandler, R. E., Kendon, E. J., Wid-  
738 mann, M., ... Thiele-Eich, I. (2010, 9). Precipitation downscaling under  
739 climate change: Recent developments to bridge the gap between dynami-  
740 cal models and the end user. *Reviews of Geophysics*, 48(3), RG3003. doi:  
741 10.1029/2009RG000314
- Matiu, M., & Hanzer, F. (2022, 6). Bias adjustment and downscaling of snow cover  
743 fraction projections from regional climate models using remote sensing for the  
744 European Alps. *Hydrology and Earth System Sciences*, 26(12), 3037–3054. doi:  
745 10.5194/hess-26-3037-2022
- Maurer, E. P., & Pierce, D. W. (2014, 3). Bias correction can modify climate  
747 model simulated precipitation changes without adverse effect on the en-  
748 semble mean. *Hydrology and Earth System Sciences*, 18(3), 915–925. doi:  
749 10.5194/hess-18-915-2014
- McMillan, H. K., Gnann, S. J., & Araki, R. (2022, 6). Large Scale Evaluation of Re-  
751 lationships Between Hydrologic Signatures and Processes. *Water Resources Re-  
752 search*, 58(6). doi: 10.1029/2021WR031751
- Melsen, L. A., Addor, N., Mizukami, N., Newman, A. J., Torfs, P. J., Clark, M. P.,  
754 ... Teuling, A. J. (2018). Mapping (dis)agreement in hydrologic projections.

- 756                   *Hydrology and Earth System Sciences*. doi: 10.5194/hess-22-1775-2018  
 757     Melsen, L. A., Teuling, A. J., Torfs, P. J., Zappa, M., Mizukami, N., Mendoza,  
 758       P. A., ... Uijlenhoet, R. (2019, 1). Subjective modeling decisions can sig-  
 759       nificantly impact the simulation of flood and drought events. *Journal of*  
 760       *Hydrology*, 568, 1093–1104. doi: 10.1016/J.JHYDROL.2018.11.046  
 761     Mendoza, P. A., Clark, M. P., Mizukami, N., Gutmann, E. D., Arnold, J. R.,  
 762       Brekke, L. D., & Rajagopalan, B. (2016). How do hydrologic modeling de-  
 763       cisions affect the portrayal of climate change impacts? *Hydrological Processes*.  
 764       doi: 10.1002/hyp.10684  
 765     Meyer, J., Kohn, I., Stahl, K., Hakala, K., Seibert, J., & Cannon, A. J. (2019, 3).  
 766       Effects of univariate and multivariate bias correction on hydrological impact  
 767       projections in alpine catchments. *Hydrology and Earth System Sciences*, 23(3),  
 768       1339–1354. doi: 10.5194/hess-23-1339-2019  
 769     O'Neill, B. C., Tebaldi, C., van Vuuren, D. P., Eyring, V., Friedlingstein, P., Hurtt,  
 770       G., ... Sanderson, B. M. (2016, 9). The Scenario Model Intercomparison  
 771       Project (ScenarioMIP) for CMIP6. *Geoscientific Model Development*, 9(9),  
 772       3461–3482. doi: 10.5194/gmd-9-3461-2016  
 773     Oudin, L., Hervieu, F., Michel, C., Perrin, C., Andréassian, V., Anctil, F., &  
 774       Loumagne, C. (2005, 3). Which potential evapotranspiration input for a  
 775       lumped rainfall-runoff model? *Journal of Hydrology*, 303(1-4), 290–306. doi:  
 776       10.1016/j.jhydrol.2004.08.026  
 777     Pierce, D. W., Cayan, D. R., Maurer, E. P., Abatzoglou, J. T., & Hegewisch, K. C.  
 778       (2015, 12). Improved Bias Correction Techniques for Hydrological Simulations  
 779       of Climate Change\*. *Journal of Hydrometeorology*, 16(6), 2421–2442. doi:  
 780       10.1175/JHM-D-14-0236.1  
 781     Rastogi, D., Kao, S., & Ashfaq, M. (2022, 8). How May the Choice of Downscaling  
 782       Techniques and Meteorological Reference Observations Affect Future Hydrocli-  
 783       mate Projections? *Earth's Future*, 10(8). doi: 10.1029/2022EF002734  
 784     Reiter, P., Gutjahr, O., Schefczyk, L., Heinemann, G., & Casper, M. (2018, 3). Does  
 785       applying quantile mapping to subsamples improve the bias correction of daily  
 786       precipitation? *International Journal of Climatology*, 38(4), 1623–1633. doi:  
 787       10.1002/joc.5283  
 788     Ruffault, J., Martin-StPaul, N. K., Duffet, C., Goge, F., & Mouillot, F. (2014, 7).  
 789       Projecting future drought in Mediterranean forests: bias correction of climate  
 790       models matters! *Theoretical and Applied Climatology*, 117(1-2), 113–122. doi:  
 791       10.1007/s00704-013-0992-z  
 792     Sawicz, K., Wagener, T., Sivapalan, M., Troch, P. A., & Carrillo, G. (2011). Catch-  
 793       ment classification: empirical analysis of hydrologic similarity based on catch-  
 794       ment function in the eastern USA. *Hydrology and Earth System Sciences*  
 795       Discussions. doi: 10.5194/hessd-8-4495-2011  
 796     Sepúlveda, U. M., Mendoza, P. A., Mizukami, N., & Newman, A. J. (2022, 7).  
 797       Revisiting parameter sensitivities in the variable infiltration capacity model  
 798       across a hydroclimatic gradient. *Hydrology and Earth System Sciences*, 26(13),  
 799       3419–3445. doi: 10.5194/hess-26-3419-2022  
 800     Stoner, A. M., Hayhoe, K., Yang, X., & Wuebbles, D. J. (2013). An asynchronous  
 801       regional regression model for statistical downscaling of daily climate variables.  
 802       *International Journal of Climatology*. doi: 10.1002/joc.3603  
 803     Switanek, M. B., Troch, P. A., Castro, C. L., Leuprecht, A., Chang, H.-I., Mukher-  
 804       jee, R., & Demaria, E. M. C. (2017, 6). Scaled distribution mapping:  
 805       a bias correction method that preserves raw climate model projected  
 806       changes. *Hydrology and Earth System Sciences*, 21(6), 2649–2666. doi:  
 807       10.5194/hess-21-2649-2017  
 808     Taylor, K. E. (2001, 4). Summarizing multiple aspects of model performance in  
 809       a single diagram. *Journal of Geophysical Research: Atmospheres*, 106(D7),  
 810       7183–7192. doi: 10.1029/2000JD900719

- 811 Teng, J., Potter, N. J., Chiew, F. H. S., Zhang, L., Wang, B., Vaze, J., & Evans,  
 812 J. P. (2015, 2). How does bias correction of regional climate model precipi-  
 813 tation affect modelled runoff? *Hydrology and Earth System Sciences*, 19(2),  
 814 711–728. doi: 10.5194/hess-19-711-2015
- 815 Teutschbein, C., & Seibert, J. (2010, 7). Regional Climate Models for Hy-  
 816 drological Impact Studies at the Catchment Scale: A Review of Recent  
 817 Modeling Strategies. *Geography Compass*, 4(7), 834–860. doi: 10.1111/  
 818 j.1749-8198.2010.00357.x
- 819 Vano, J. A., Kim, J. B., Rupp, D. E., & Mote, P. W. (2015). Selecting climate  
 820 change scenarios using impact-relevant sensitivities. *Geophysical Research Let-  
 821 ters*. doi: 10.1002/2015GL063208
- 822 Vásquez, N., Cepeda, J., Gómez, T., Mendoza, P. A., Lagos, M., Boisier, J. P.,  
 823 ... Vargas, X. (2021). Catchment-Scale Natural Water Balance in Chile.  
 824 In (pp. 189–208). Retrieved from [http://link.springer.com/10.1007/978-3-030-56901-3\\_9](http://link.springer.com/10.1007/978-3-030-56901-3_9) doi: 10.1007/978-3-030-56901-3{\\_}9
- 825 Vicuña, S., Vargas, X., Boisier, J. P., Mendoza, P. A., Gómez, T., Vásquez, N., &  
 826 Cepeda, J. (2021). Impacts of Climate Change on Water Resources in Chile.  
 827 In B. Fernández & J. Gironás (Eds.), *Water resources of chile* (pp. 347–363).  
 828 Cham: Springer International Publishing. Retrieved from [https://doi.org/10.1007/978-3-030-56901-3\\_19](https://doi.org/10.1007/978-3-030-56901-3_19) doi: 10.1007/978-3-030-56901-3{\\_}19
- 829 Vogel, E., Johnson, F., Marshall, L., Bende-Michl, U., Wilson, L., Peter, J. R.,  
 830 ... Duong, V. C. (2023, 7). An evaluation framework for downscaling and  
 831 bias correction in climate change impact studies. *Journal of Hydrology*, 622,  
 832 129693. doi: 10.1016/j.jhydrol.2023.129693
- 833 Vrac, M., & Thao, S. (2020, 11). R2D2; v2.0: accounting for temporal dependences  
 834 in multivariate bias correction via analogue rank resampling. *Geoscientific  
 835 Model Development*, 13(11), 5367–5387. doi: 10.5194/gmd-13-5367-2020
- 836 Wan, Z. (2014, 1). New refinements and validation of the collection-6 MODIS land-  
 837 surface temperature/emissivity product. *Remote Sensing of Environment*, 140,  
 838 36–45. doi: 10.1016/j.rse.2013.08.027
- 839 Werner, A. T., & Cannon, A. J. (2016, 4). Hydrologic extremes – an intercompar-  
 840 ison of multiple gridded statistical downscaling methods. *Hydrology and Earth  
 841 System Sciences*, 20(4), 1483–1508. doi: 10.5194/hess-20-1483-2016
- 842 Widmann, M., Bretherton, C. S., & Salathé, E. P. (2003, 3). Statistical Precipi-  
 843 tation Downscaling over the Northwestern United States Using Numerically  
 844 Simulated Precipitation as a Predictor\*. *Journal of Climate*, 16(5), 799–816.  
 845 doi: 10.1175/1520-0442(2003)016<0799:SPDOTN>2.0.CO;2
- 846 Wilby, R. L., & Dessai, S. (2010). Robust adaptation to climate change. *Weather*.  
 847 doi: 10.1002/wea.543
- 848 Woods, R. A. (2009, 10). Analytical model of seasonal climate impacts on snow hy-  
 849 drology: Continuous snowpacks. *Advances in Water Resources*, 32(10), 1465–  
 850 1481. doi: 10.1016/j.advwatres.2009.06.011
- 851 Wootten, A. M., Dixon, K. W., Adams-Smith, D. J., & McPherson, R. A. (2021,  
 852 2). Statistically downscaled precipitation sensitivity to gridded observation  
 853 data and downscaling technique. *International Journal of Climatology*, 41(2),  
 854 980–1001. doi: 10.1002/joc.6716
- 855 Wu, Y., Miao, C., Fan, X., Gou, J., Zhang, Q., & Zheng, H. (2022, 11). Quantify-  
 856 ing the Uncertainty Sources of Future Climate Projections and Narrowing  
 857 Uncertainties With Bias Correction Techniques. *Earth's Future*, 10(11). doi:  
 858 10.1029/2022EF002963
- 859 Xavier, A. C. F., Martins, L. L., Rudke, A. P., de Morais, M. V. B., Martins, J. A.,  
 860 & Blain, G. C. (2022, 1). Evaluation of Quantile Delta Mapping as a bias-  
 861 correction method in maximum rainfall dataset from downscaled models in São  
 862 Paulo state (Brazil). *International Journal of Climatology*, 42(1), 175–190.  
 863 doi: 10.1002/joc.7238